Optical sensing of aqueous nitrate anion by a platinum(II) triimine salt based solid state material

Amie E. Norton,[I,†*] Mahmood K. Abdolmaleki,[I,I] Logan Andriot,[I] Christina Cashen,[I] Jeanette A. Krause,[I] William B. Connick[I†] and Sayandev Chatterjee[‡*]
[I]Department of Chemistry, University of Cincinnati, Cincinnati, OH 45221, United States of America
[†]Present address: Department of Entomology, Kansas State University, Manhattan, KS 66503, United States of America
[I]Present address: Department of Biology and Chemistry, Texas A&M International University, Laredo, TX, 78041, United States of America
[‡]TerraPower LLC, Bellevue, WA 98008, United States of America
Email: amien@ksu.edu, schatterjee@terrapower.com

†This work is dedicated to William B. Connick, who passed away in April 2018

Supporting Information Placeholder

ABSTRACT: Selective and quantitative measurement of aqueous nitrate (NO_3^-) anion is achieved using solid [Pt(Cl-4-tpy)Cl]ClO_4 salt (Cl-4-tpy = 4-chloro-2,2′:6′2″-terpyridine) as is, and as the salt supported on controlled porous glass. This detection method relies on the color change of the Pt(II) complex from yellow to red and intense luminescence response upon ClO_4^- exchange with NO_3^- due to concomitant enhancement of Pt•••Pt interactions. The spectroscopic response is highly selective for NO_3^- over a large range of halides and oxoanions.

The selective and sensitive detection of specific anions for the monitoring and assessment of water quality remains a global environmental and chemical challenge.[1,2] One such example is the nitrate (NO_3^-) anion; it has widespread use in munitions/explosives manufacturing and chemical fertilizer preparation,[3–5] and an abundance of nitrate found in livestock as well as organic wastes[6] has led to groundwater and food supply contamination and raised public health concerns. Epidemiologic studies have associated continued NO_3^- exposure via ingestion to multiple medical issues that include spontaneous abortions in pregnant women,[7] birth defects of the central nervous system and intrauterine growth restriction in children,[8] and cardiovascular effects[9] and gastric cancer in adults.[10] According to recent World Health Organization (WHO) reports, NO_3^- concentrations in surface waters have increased significantly over the last 30 – 40 years,[11] emphasizing a growing need for its rapid *in situ* detection and prompting the United States Environmental Protection Agency (US-EPA) to set the ambient water quality limit of NO_3^- at 10 ppm.[12]

Current EPA strategies for aqueous NO_3^- detection involve ion selective electrode based potentiometry[13] or *in-situ* NO_3^- reduction followed by NO_2^- colorimetry. Alternate methods proposed for *in-situ* NO_3^- detection include UV-spectroscopy,[13] ion chromatography,[14] and capillary electrophoresis.[15] These proposed techniques suffer from limitations including imperfect selectivity, longer processing times, complicated and expensive instrumentation, or need for processing expertise. This impacts rapid testing and impedes water quality assessment particularly in remote corners of the globe where such timely testing can be critical. An elegant study by Daniel et al. relied on two-step sensing of nitrate utilizing an initial enzymatic reduction of NO_3^- to NO_2^- followed by colorimetric detection of the NO_2^- using functionalized Au nanoparticles.[16] While this technique offers a selective, sensitive, and robust method for rapid *in-situ* NO_2^-/NO_3^-, the need for multiple processing steps makes it less than ideal in terms of operational flexibility for on-site deployment.

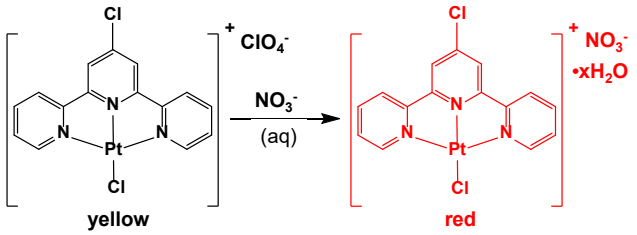

Scheme 1. Conversion of yellow [Pt(Cl-4-tpy)Cl]ClO_4 (**1**•ClO_4) to red [Pt(Cl-4-tpy)Cl]NO_3•xH_2O (**1**•NO_3•xH_2O) upon exposure to aqueous NO_3^-.

We have recently demonstrated a new method of colorimetric aqueous NO_3^- detection, complemented by a second and more sensitive luminescent mode.[17] This method utilizes solid-state hybrid materials based on square-planar platinum(II) salts supported on mesoporous silica.[18] The strategy relies on selective recognition of the aqueous NO_3^- anion by a square-planar Pt(II) salt, which results in changes in the extended solid-state lattice structure upon anion exchange. Square-planar, coordinately-unsaturated Pt(II) complexes with sterically permitting ligands demonstrate rich spectroscopic properties that are modulated by changing the Pt•••Pt interactions.[1,19–21] Incorporation of an anion guest into the crystal lattice that can significantly alter the Pt•••Pt interactions in a desired way, triggers correlated changes in the electronic structure of the Pt(II) compound. This is reflected in vivid changes in their optical spectroscopies.[1,2,17] Our previous aqueous NO_3^- detection method required adjusting the pH of the material to <0. Herein, we present a new Pt(II) salt, [Pt(Cl-4-tpy)Cl]ClO_4 (**1**•ClO_4), which shows a unique optical response to aqueous NO_3^- anion without the need for pH adjustment. This simplifies the detection process for on-site applications and expands the applicability of the new Pt(II) salt to broader matrices.

To assess the colorimetric response of **1**•ClO_4, either yellow microcrystalline powders (~10 mg) or an aqueous suspension (~10 mg/mL) were exposed to aqueous NO_3^- (1 mL 1 M solution, Scheme 1). Exposure of either the solid or the suspension resulted in a distinct color change from yellow to red within 2-5 minutes.

Optical spectroscopy was used to corroborate the visual color changes of **1**•ClO_4 from yellow to red (Fig. **1**). Absorption spectra of microcrystalline powders of **1**•ClO_4 dispersed on a glass slide exhibit spin-allowed intra-ligand (π-π*) transitions at wavelengths below 365 nm. In addition, a broad low-energy absorption band at wavelengths between 365 and 450 nm is assigned to the $d\pi$(Pt)–π(Cl-4-tpy) metal-to-ligand charge transfer (MLCT) transition of the Pt(Cl-4-tpy)Cl^+ chromophore *vide-infra*.[22] Immersion of the glass slide with dispersed **1**•ClO_4 microcrystals into a 1.0 mM aqueous NO_3^- solution results in the appearance of a new band at longer wavelengths. This new band is nearly identical to that observed for an independently synthesized **1**•NO_3•$2H_2O$ sample. Based on comparison with similar Pt(II) salts, this low-energy band is attributed to a metal–metal-to-ligand charge-transfer MMLCT transition [$d\sigma^*$(Pt)–π^*(Cl-4-tpy)] where the $d\sigma^*$ arises from the interaction of the d_{z^2}(Pt) orbitals of adjacent complexes, which in turn is suggestive of extended Pt•••Pt interactions.[2,20,22–24]

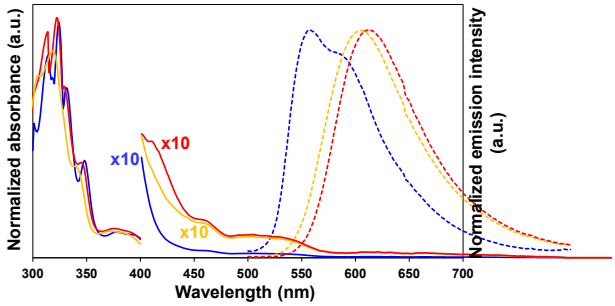

Fig. 1. Optical spectra of **1**•ClO_4 (blue lines) and **1**•NO_3•$2H_2O$ (red lines); spectra of **1**•ClO_4 post exposure to aqueous NO_3^- (yellow lines); solid lines represent absorption and dashed lines represent emission (λ_{ex} = 436 nm).

On the other hand, the emission spectrum (λ_{ex} = 436 nm) shows a characteristic asymmetric emission band maximizing near 557 nm (dashed blue line in Fig. 1) with a shoulder at 590 nm. The emission for **1**•NO_3 is red-shifted showing a new emission maximum at 617 nm (dashed red line). When **1**•ClO_4 was exposed to 1.0 mM aqueous NO_3^- solution, a similar new band was observed at 608 nm (dashed yellow line). As in the case of the absorption spectra, the new band at lower energy is attributed to a metal–metal-to-ligand charge-transfer MMLCT transition, further supporting extended Pt•••Pt interactions in both **1**•NO_3 and **1**•ClO_4 post aqueous NO_3^- exposure. We have previously shown that nano-structured platforms with high surface area (e.g. controlled porous glass (CPG) beads of pore sizes 383 Å) respond more rapidly.[17,18] Aqueous NO_3^- exposure of **1**•ClO_4 encapsulated in the CPGs (**1**•ClO_4@CPG-383) produced similar optical changes, albeit with the expected faster response times, which is attributed to the surface area of the sample in the nano-structured environment.

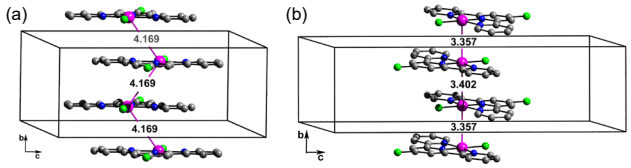

Fig. 2. Packing arrangements for (a) **1**•ClO_4 and (b) **1**•NO_3•$2H_2O$ (ClO_4^- and NO_3^-•$2H_2O$ units omitted for clarity). Distances are shown in Å.

The colorimetric and luminescent changes in **1**•ClO_4 upon exposure to aqueous NO_3^- suggests an alteration of the nearest neighbor Pt•••Pt interactions. One explanation for the observed changes is the incorporation of NO_3^- ions within the lattice as ClO_4^- is displaced. This anion replacement presumably perturbs stacking in the square planar Pt(II) units, and consequently alters the lowest lying MMLCT energy; this is expressed in the color and luminescence changes in the material.[20,25,26] Structural studies were undertaken to test this hypothesis and gain insight into the Pt•••Pt interactions.

Single crystal X-ray structures were determined for independently synthesized **1**•ClO_4 and **1**•NO_3•$2H_2O$ salts (Fig. **S1**, Tables **S2**-**S4**). Yellow crystals of **1**•ClO_4, grown from a 1:1 water:acetone solution, show a lattice devoid of solvent and consisting of equally-spaced cations with long Pt•••Pt interaction distances, 4.169(3)Å, and highly-bent Pt•••Pt•••Pt angles, 106.28(1)° (Fig. **2**).[27] In contrast, orange-red crystals of **1**•NO_3•$2H_2O$, grown from acetone-HNO_3 solution, show incorporation of 2 molecules of water in the lattice. The nearest neighbor Pt•••Pt distances are shortened and alternate between 3.3570(4)Å and 3.4018(4)Å and the Pt•••Pt•••Pt angle is essentially linear, 172.66(1)° (Fig. **2**).[28]

Powder X-ray diffraction (PXRD) measurements corroborate identification of the species generated during exposure of **1**•ClO_4 to aqueous NO_3^- for a specified length of time, and therefore provides mechanistic insight. The diffractogram of powdered **1**•ClO_4 measured post exposure to aqueous NO_3^- for 1 hour shows peaks of the starting **1**•ClO_4 complex in addition to a set of new broad peaks. While retention of the parent peaks indicates incomplete conversion, the new peaks match the simulated diffraction pattern from **1**•NO_3•$2H_2O$ single crystals (Fig. **S2**). Thus, it can be concluded that exposure of **1**•ClO_4 to aqueous NO_3^- anions leads to the substitution of the ClO_4^- with NO_3^- within the lattice structure.

To determine the structural fate of the complexes upon incorporation within the CPG, diffractograms were recorded on both **1**•ClO_4@CPG-383 and **1**•NO_3•$2H_2O$@CPG-383 samples (Fig. **S2**). Both species are characterized by broad, amorphous silica peaks at 2θ = 21°, along with several additional features. For the **1**•ClO_4@CPG-383 composite, the additional features match diffraction peaks in the pristine **1**•ClO_4 sample. Similarly, the additional features observed for **1**•NO_3•$2H_2O$@ CPG-383 also match the pristine **1**•NO_3•$2H_2O$ peaks. This indicates that for both composites, the structural integrity of the starting Pt(II) salts remains preserved even after incorporation into the CPGs. Exposure of **1**•ClO_4@CPG-383 to aqueous NO_3^- results in $ClO_4^- \rightarrow NO_3^-$ anion exchange as demonstrated by the PXRD profile showing peaks from both the starting complex as well as the freshly generated **1**•NO_3•$2H_2O$@ CPG-383 species. Similar to previous studies,[18] scanning electron micrographs of **1**•ClO_4@CPG-383 show microcrystalline deposits rich in Pt covering the CPG surface (Fig. **S4**). In magnified transmission

electron micrographs, the microcrystals appear as hexagonal elongated rods with a tendency to aggregate upon contact with aqueous NO_3^- (Fig. **S5**). A more detailed analysis is presently underway.

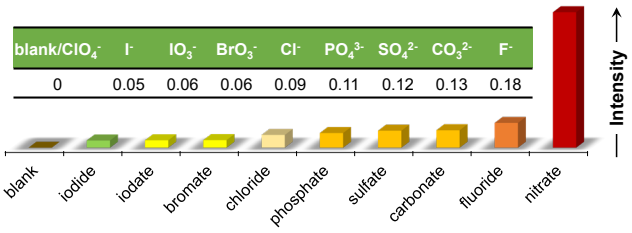

Fig. 3. The emission intensity responses of the **1**•ClO_4@CPG-383 composite post exposure to various anions

To qualitatively determine the selectivity for the NO_3^- anion over other anionic species, powdered **1**•ClO_4 was loaded onto CPG-383 beads (0.2 g, 2 wt% **1**•ClO_4 @CPG-383) and separately exposed to a range of 1.0 M aqueous solutions of I^-, IO_3^-, BrO_3^-, Cl^-, PO_4^{3-}, SO_4^{2-}, CO_3^{2-}, and F^- for 1 h. These anions were chosen as they are key anions present in environmental water matrices. The emission intensities (λ_{ex} = 532 nm) of the exposed CPGs were compared with CPGs exposed to 10^{-3} M NO_3^- for the same time period. Because practical matrices are expected to contain an overwhelming excess of interfering species compared to the target species, the concentrations of the interfering anions were deliberately chosen to be four orders of magnitude greater than aqueous NO_3^- concentrations with the objective of demonstrating the uniqueness of the targeted response of **1**•ClO_4@CPG to the NO_3^- anion. The emission intensity responses of the **1**•ClO_4@CPG-383 composite post exposure to various anions is shown in Fig. **3**. As can be seen, there is an overwhelming response of the composite towards aqueous NO_3^-. The selectivity factor for the interfering anions (calculated as the ratio of the maximum emission intensities observed in the presence of interfering anions to that observed in the presence of NO_3^-) range from 0.05 for I^- to 0.18 for F^-, confirming the high selectivity of **1**•ClO_4 for NO_3^- anion (Fig. **3**, inset, Fig. **S4**).

Luminescence spectroscopy was used for the NO_3^- quantification.[1,21] In the test, equal amounts of **1**•ClO_4@CPG-383 were exposed to aqueous solutions with different NO_3^- concentrations (1 mL of 10^{-4} to 1 M). Three independent measurements were conducted for each concentration. Upon excitation at 532 nm, **1**•ClO_4@CPG-383 showed a weak asymmetric emission (λ_{max} = 566 nm) with a shoulder at 604 nm, prior to NO_3^- exposure. Upon exposure to 10^{-4} M aqueous NO_3^- for 15 mins, a broader asymmetric band centered at ~610 nm was observed with a ~7-fold increase in emission intensity (Fig. **4**a). Further addition of aqueous NO_3^- (in 0.1 mL aliquots until 0.1 M) resulted in an increase in intensity (Fig. **4**a), and an emission maximum shifted to higher wavelength until a maximum was reached at 620 nm. The emission band also narrows at higher NO_3^- concentrations suggestive of an equilibrium shift to a single platinum species. The logarithm of luminescence intensity of the respective emission maxima was observed to increase linearly with the logarithm of nitrate concentration (Fig. **4**b).

The limit of detection (LOD) was calculated from the log-log plot based on the IUPAC recommended Equation 1 reported by Long et al.[29]

$$DL = \frac{k \bullet S_b}{m} \qquad [1]$$

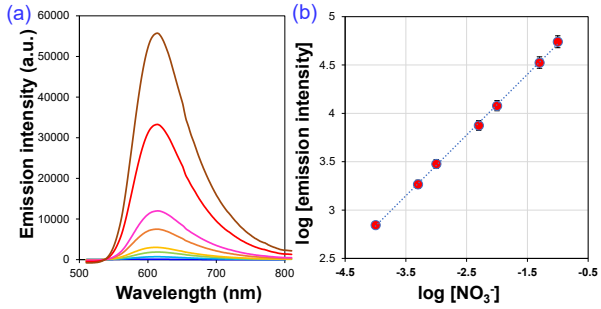

Fig. 4. (a) Luminescence spectra of **1**•ClO_4@CPG-383 upon exposure to varying concentrations of aqueous NO_3^- for 1 hour: (——) 0 M, (——) 10^{-4} M, (——) 5×10^{-4} M, (——) 10^{-3} M, (——) 5×10^{-3} M, (——) 10^{-2} M, (——) 5×10^{-2} M, (——) 10^{-1} M (λ_{ex}= 532 nm), (b) logarithmic plot of the maximum emission intensity (λ_{max}= 605 nm) of **1**•ClO_4@CPG-383 versus the concentration of solution NO_3^- in solution.

Here, DL is the detection limit, k is a numerical constant, m is the slope of the linear region of the plot, and S_b is the standard error for the blank measurements. Per IUPAC recommendations, a k value of 3 was applied, which corresponds to a 99.87% confidence level. Based on this, a detection limit of 0.046±0.005 mM (2.85±0.31 ppm) is obtained, significantly lower than the ambient water quality limit of 0.16 mM (10 ppm) set by US-EPA.

The ability of the **1**•ClO_4@CPG-383 composite to detect aqueous NO_3^- from a complex multicomponent matrix was tested using groundwater samples spiked with varying concentrations of NO_3^- via standard additions such that the cumulative NO_3^- concentrations ranged from 5×10^{-3} to 7.5×10^{-2} M, as determined by independent ion chromatography (IC) measurements. Although the emission profile is observed to be broader as compared to DI water, a proportional rise in emission intensity with increase in NO_3^- concentrations was observed (Fig. **S5**, left panel). The logarithm of luminescence intensity of the respective emission maxima showed a linear increase with the logarithm of total nitrate concentration (Fig. **S5**, right panel), similar to DI water. The slope of the response in the groundwater differs from that of DI water, presumably the groundwater matrix perturbs the electronic structure of the **1**•ClO_4 salt differently. Despite the differences, it is possible to determine the NO_3^- concentration from the log-log plot. The NO_3^- concentration in groundwater was determined to be 4.4±0.3 mM, consistent with a value of 5.1 mM as determined from independent IC measurements.

This investigation demonstrates the use of a solid-state material for the unambiguous rapid and selective detection of NO_3^- in aqueous solution without the requirement of additives and offers the potential for a new sensor compatible with field deployment. The accumulated evidence establishes that the colorimetric and luminescence response of **1**•ClO_4 to aqueous NO_3^- is a consequence of a contraction of the intermolecular Pt•••Pt distances exhibiting stronger interactions that results from ClO_4^-/NO_3^- anion exchange. It is assumed that the energy requirements for the molecular rearrangement is compensated by the non-covalent interactions in **1**$\cdot NO_3 \cdot 2H_2O$. This is presumably due to the steric and electronic complementarity of **1** $\cdot ClO_4$ towards aqueous NO_3^- anions making this salt suitable for NO_3^- sensing. It is worth acknowledging that in the vast lit-

erature on luminescent Pt(II) complexes, there might be additional salts with similar attributes that are also optimally suitable for NO_3^- sensing.

This research was supported by NSF CHE-1152853, US EPA STAR, FP-91765901 to A.E.N., and the Laboratory Directed Research and Development Program at the Pacific Northwest National Laboratory (PNNL) to S.C. PNNL is operated by Battelle for the U.S. DOE under Contract DE-AC05-76RL01830. Single crystal data was collected through SCrALS, Beamline 11.3.1, Advanced Light Source (ALS), Lawrence Berkeley National Laboratory. ALS is supported by the U.S. DOE, Office of Energy Sciences Materials Sciences Division, under Contract DE-AC02-05CH11231. We thank Dr. Garry Hanon for helping with resources.

Conflicts of interest

There are no conflicts to declare.

Notes and references

1 S. Chatterjee, A. E. Norton, M. K. Edwards, J. M. Peterson, S. D. Taylor, S. A. Bryan, A. Andersen, N. Govind, T. E. Albrecht-Schmitt, W. B. Connick and T. G. Levitskaia, *Inorg. Chem.*, 2015, **54**, 9914–9923.

2 S. D. Taylor, W. Howard, N. Kaval, R. Hart, J. A. Krause and W. B. Connick, *Chem. Commun.*, 2010, **46**, 1070–1072.

3 G. A. Blanco, Y. H. Nai, E. F. Hilder, R. A. Shellie, G. W. Dicinoski, P. R. Haddad and M. C. Breadmore, *Anal. Chem.*, 2011, **83**, 9068–9075.

4 J. J. Brady, P. M. F. Iv, J. J. Perez, E. J. Judge and R. J. Levis, in *Chemical, Biological, Radiological, Nuclear, and Explosives (CBRNE) Sensing XIII*, SPIE, 2012, vol. 8358, pp. 242–250.

5 B. Yellampelle, M. Sluch, S. Asher and B. Lemoff, in *Chemical, Biological, Radiological, Nuclear, and Explosives (CBRNE) Sensing XII*, SPIE, 2011, vol. 8018, pp. 353–359.

6 D. Castro-Herrera, K. Prost, Y. Schäfer, D.-G. Kim, F. Yimer, M. Tadesse, M. Gebrehiwot and N. Brüggemann, *J. Environ. Qual.*, 2022, **51**, 19–32.

7 F. Raffaelli, L. Nanetti, A. Vignini, L. Mazzanti, S. R. Giannubilo, C. M. Curzi, A. Turi, P. Vitali and A. L. Tranquilli, *Fertil. Steril.*, 2010, **93**, 1976–1982.

8 M. Rhoades, D. Barnes-Josiah, R. Spalding, L. Howard, C. Steele and C. Beseler, *Child Health Res. Inst. Pediatr. Res. Forum*.

9 L. Wang, Z. Fu, J. Zheng, S. Wang, Y. Ping, B. Gao, X. Mo, P. Liang and J. Huang, *Ecotoxicol. Environ. Saf.*, 2022, **230**, 113161.

10 R. Picetti, M. Deeney, S. Pastorino, M. R. Miller, A. Shah, D. A. Leon, A. D. Dangour and R. Green, *Environ. Res.*, 2022, **210**, 112988.

11 M. J. Hill, *Nitrates and Nitrites in Food and Water*, CRC Press, 1996.

12 B. Daniels, N. Mesner, 2010. Nitrate. *Utah State University: Water Quality Extension. Utah State University, Logan, Utah.*

13 J. Ma, F. Meng, Y. Zhou, Y. Wang and P. Shi, *Sensors*, 2018, **18**, 606.

14 J. M. Doyle, M. L. Miller, B. R. McCord, D. A. McCollam and G. W. Mushrush, *Anal. Chem.*, 2000, **72**, 2302–2307.

15 A. Beutner, B. Scherer and F.-M. Matysik, *Talanta*, 2018, **183**, 33–38.

16 W. L. Daniel, M. S. Han, J.-S. Lee and C. A. Mirkin, *J. Am. Chem. Soc.*, 2009, **131**, 6362–6363.

17 A. E. Norton, M. Sharma, C. Cashen, M.-A. Dourges, T. Toupance, J. A. Krause, R. K. Motkuri, W. B. Connick and S. Chatterjee, *ACS Appl. Mater. Interfaces*, 2021, **13**, 16197–16209.

18 A. E. Norton, K. P. S. Zanoni, M.-A. Dourges, L. P. Ravaro, M. K. Abdolmaleki, A. S. S. de Camargo, T. Toupance, W. B. Connick and S. Chatterjee, *J. Mater. Chem. C*, 2021, **9**, 6193–6207.

19 L. J. Grove, A. G. Oliver, J. A. Krause and W. B. Connick, *Inorg. Chem.*, 2008, **47**, 1408–1410.

20 J. A. Bailey, M. G. Hill, R. E. Marsh, V. M. Miskowski, W. P. Schaefer and H. B. Gray, *Inorg. Chem.*, 1995, **34**, 4591–4599.

21 A. E. Norton, M. Karimi Abdolmaleki, J. Liang, M. Sharma, R. Golsby, A. Zoller, J. A. Krause, W. B. Connick and S. Chatterjee, *Chem. Commun.*, 2020, **56**, 10175–10178.

22 P. Du, *Inorganica Chim. Acta*, 2010, **363**, 1355–1358.

23 S. D. Taylor, A. E. Norton, R. T. Hart, M. K. Abdolmaleki, J. A. Krause and W. B. Connick, *Chem. Commun.*, 2013, **49**, 9161–9163.

24 A. E. Norton, M. K. Abdolmaleki, J. M. Ringo, V. M. Shingade, C. Cashen, M. Sharma, W. B. Connick and S. Chatterjee, *Sens. Actuators B Chem.*, 2021, **329**, 129207.

25 K. Zhang, M. C.-L. Yeung, S. Y.-L. Leung and V. W.-W. Yam, *ACS Appl. Mater. Interfaces*, 2020, **12**, 8503–8512.

26 J. S. Field, J.-A. Gertenbach, R. J. Haines, L. P. Ledwaba, N. T. Mashapa, D. R. McMillin, O. Q. Munro and G. C. Summerton, *Dalton Trans.*, 2003, 1176–1180.

27 J. A. Krause, L. Androit, A. E. Norton, W. B. Connick, CCDC-2170160, *CSD Communications*, 2022, DOI: 10.5517/ccdc.csd.cc2bv75m.

28 J. A. Krause, L. Androit, A. E. Norton, W. B. Connick, CCDC-2170168, *CSD Communications*, 2022, DOI: 10.5517/ccdc.csd.cc2bv7fw.

29 G. L. Long and J. D. Winefordner, *Anal. Chem.*, 1983, **55**, 712A-724A.